2018-06-15

Time domain diffuse correlation spectroscopy: modeling the effects of laser coherence length and instrument response function

Xiaojun Cheng, Davide Tamborini, Stefan A Carp, Oleg Shatrovoy, Bernhard Zimmerman, Danil Tyulmankov, Andrew Siegel, Megan Blackwell, Maria Angela Franceschini, David A Boas. 2018. "Time domain diffuse correlation spectroscopy: modeling the effects of laser coherence length and instrument response function." OPTICS LETTERS, Volume 43, Issue 12, pp. 2756 - 2759 (4). https://doi.org/10.1364/OL.43.002756

https://hdl.handle.net/2144/37732

HHS Public Access
Author manuscript
Opt Lett. Author manuscript; available in PMC 2019 June 15.

Published in final edited form as:
Opt Lett. 2018 June 15; 43(12): 2756–2759.

Time domain diffuse correlation spectroscopy: modeling the effects of laser coherence length and instrument response function

XIAOJUN CHENG[1,2,*], **DAVIDE TAMBORINI**[2], **STEFAN A. CARP**[2], **OLEG SHATROVOY**[3], **BERNHARD ZIMMERMAN**[1,2], **DANIL TYULMANKOV**[2], **ANDREW SIEGEL**[3], **MEGAN BLACKWELL**[3], **MARIA ANGELA FRANCESCHINI**[2], and **DAVID A. BOAS**[1,2]

[1]Neurophotonics Center, Department of Biomedical Engineering, Boston University, Massachusetts 02215, USA

[2]Optics Division at the Athinoula A. Martinos Center for Biomedical Imaging, Department of Radiology, Massachusetts General Hospital and Harvard Medical School, Charlestown, Massachusetts 02129, USA

[3]MIT Lincoln Laboratory, Lexington, Massachusetts 02421, USA

Abstract

Diffuse correlation spectroscopy (DCS) is an optical technique that non-invasively quantifies an index of blood flow (BF_i) by measuring the temporal autocorrelation function of the intensity fluctuations of light diffusely remitted from the tissue. Traditional DCS measurements use continuous wave (CW) lasers with coherence lengths longer than the photon path lengths in the sample to ensure that the diffusely remitted light is coherent and generates a speckle pattern. Recently, we proposed time domain DCS (TD-DCS) to allow measurements of the speckle fluctuations for specific path lengths of light through the tissue, which has the distinct advantage of permitting an analysis of selected long path lengths of light to improve the depth sensitivity of the measurement. However, compared to CW-DCS, factors including the instrument response function (IRF), the detection gate width, and the finite coherence length need to be considered in the model analysis of the experimental data. Here we present a TD-DCS model describing how the intensity autocorrelation functions measured for different path lengths of light depend on the coherence length, pulse width of the laser, detection gate width, IRF, BF_is and optical properties of the scattering sample. Predictions of the model are compared with experimental results using a homogeneous liquid phantom sample that mimics human tissue optical properties. The BF_is obtained from the TDDCS model for different path lengths of light agree with the BF_i obtained from CW-DCS measurements, while the standard simplified model underestimates the BF_i by a factor of ~2. This Letter establishes the theoretical foundation of the TD-DCS technique and provides guidance for future BF_i measurements in tissue.

*Corresponding author: xcheng17@bu.edu.

Keywords

(170.5280) Photon migration; (170.6920) Time-resolved imaging; (170.3660) Light propagation in tissues

---

Cerebral blood flow (CBF) is normally under tight physiological control to provide oxygen to the brain needed to maintain functional and structural integrity. Alteration in CBF puts the brain at risk for ischemia and infarction. While management of CBF is essential in neurosurgery and neurology, CBF is not routinely measured because of the lack of convenient and reliable technology. Diffuse correlation spectroscopy (DCS) offers a non-invasive way to directly and continuously measure blood flow at the bedside [1]. In DCS, a tissue of interest is illuminated by coherent near-infrared light which causes a speckle interference pattern to form by multiplying scattered light though the tissue. Dynamic scattering due to moving red blood cells causes the speckle pattern to fluctuate rapidly, and is quantified by the temporal intensity autocorrelation curve $g_w(\tau)$ of a single speckle [2–4]. The DCS-measured blood flow has been used as a biomarker of patient well-being and as an indicator of hemodynamic and metabolic functional responses [1,5–7].

The traditional DCS technique uses continuous wave (CW) light with a coherence length longer than the spread of the path length distribution of the photon trajectories. Recently, we have demonstrated the feasibility of performing DCS measurements in the time domain by using a train of laser pulses as the light source [8]. The time-gate strategy, first developed for timeresolved reflectance spectroscopy [9,10], enables measurements of autocorrelation functions at different sample times t_s corresponding to different photon path lengths. This technique has the potential of obtaining blood flow information at different penetration depths or different layers such as the skull and the brain. However, unlike CW-DCS, TD-DCS measurements are largely affected by laser pulse profiles, detector temporal response, and the coherence length which becomes comparable to the path lengths in samples. A new model is needed to handle these factors and to permit a quantitative analysis of results from TD-DCS experiments.

In this Letter, we have constructed the TD-DCS model that incorporates the instrument response function (IRF), the exposure time of the measurement described by the gate width t_{gw}, and the laser coherence length L_c into the expression of the intensity autocorrelation function g_2. The parameter $\beta=g_2(t=0)-1$, originally appearing in the Siegert relation between the intensity autocorrelation function g_2, and the field autocorrelation function $g_1, g_2 = 1 + \beta g_1^2$ [11] is shown to decrease with increasing sample timeg_1, g_2 1$t_s$and gate width$\beta g^2{}_1$ [11] is shown to decrease with increasing sample time t_s and gate width t_{gw}, which is consistent with previous experimental observations [8,12]. We have also characterized the dynamics of light scattering particles, referred to as the blood flow index BF_i, from TD-DCS measurements of a liquid phantom sample using our new model, and compared the results with both the simplistic model which does not include the effects of the IRF and L_c and with the value of BF_i obtained from CW-DCS measurements. BFis obtained from our new model agree with the BF_i obtained from the CW-DCS measurements, while the simplistic model underestimates BF_i by a factor of ~2.

Theoretically, the field autocorrelation function is [13]

$$g_1(\tau) = \langle E(0)^* E(\tau)\rangle / \langle |E(0)|\rangle^2 = \int_0^\infty P(L) g_{1L}(\tau, L)\mathrm{d}L, \quad (1)$$

where $P(L)$ is the photon path length distribution within the scattering medium, and the path length dependent field temporal autocorrelation function is

$$g_{1L}(L, \tau) = \exp\left(-\frac{1}{3}\mu_s' k_0^2 L \left\langle \Delta r^2(\tau)\right\rangle\right) = \exp\left(-2\mathrm{BF}_i \mu_s' k_0^2 L\tau\right), \quad (2)$$

where $k_0 = \frac{2\pi n}{\lambda}$ is the wavenumber of light, n is the index of refraction of the scattering medium, λ is the wavelength of light, μ_s' is the reduced scattering coefficient, and $\langle \Delta r^2(\tau)\rangle$ is the mean-square displacement of the scattering particles. Typically, in DCS measurements of blood flow, $(\Delta r^2(\tau))=6D_B\tau$, where D_B is the Brownian diffusion coefficient and is taken as the blood flow index $\mathrm{BF}_i=D_B$[14]. For a semi-infinite highly scattering medium, $P(L)$ can be calculated as [9,15]

$$P(L) = \frac{vS}{(4\pi DL/\nu)^{3/2}}\exp\left(-\mu_a L\right) \times \left[\exp\left(-\frac{z_-^2}{4DL}\right) - \exp\left(-\frac{z_+^2}{4DL}\right)\right]. \quad (3)$$

Here ρ is the source-detector distance, v is the speed of light in the sample, $z_-^2 = z_0^2 + \rho^2$, $z_+^2 = \left(z_0 + 2z_b\right)^2 + \rho^2$, $z_0 = 1/\mu_s'$, $z_b = 2D(1+R_{\mathrm{eff}})/(1 - R_{\mathrm{eff}})$, R_{eff} is the boundary reflectivity, $D = 1/\left[3\left(\mu_a + \mu_s'\right)\right]$, μ_a is the absorption, coefficient, μ_s' is the reduced scattering coefficient, and S is the normalization factor so that $\int_0^\infty P(L)\mathrm{d}L = 1$.

Ideally, the intensity autocorrelation function g_2 is related to g_1 via the Siegert relation [11]:

$$g_2(\tau) = \left\langle I(0)I(\tau)\right\rangle / \langle I(0)\rangle^2 = 1 + \beta g_1^2, \quad (4)$$

with β=1 indicating complete coherence of the detected light, and $\beta < 1$ accounting for the loss coherence and/or detection of multiple modes of light. A simplistic TD-DCS model [8,12] considers that at a detection gate sample time t_s, the path length distribution of the detected light is simply given by a Dirac δ function $P(L)$ $\delta(L= t v)$, and $g_2(t, \tau)$ can be obtained from Eqs. (2) and (4) as

$$g_2\left(t_s, \tau\right) = 1 + \beta g_{1L}^2 = 1 + \beta\exp\left(-\frac{2}{3}\mu_s' k_0^2 L\left\langle \Delta r^2(\tau)\right\rangle\right). \quad (5)$$

However, this model does not predict the correct value of BFi, as will be shown later in Fig. 3.

The effect of the finite coherence length L_c for CW sources on the autocorrelation function has been addressed by Bellini *et al.* [16], resulting in the following equation for the intensity autocorrelation function:

$$g_2(\tau) = 1 + \int_0^\infty \mathrm{d}L \int_0^\infty \mathrm{d}L' P(L) P(L') \times g_{1L}(L, \tau) g_{1L}(L', \tau) \exp\left(-2\left((L - L')/L_c\right)^2\right), \quad (6)$$

with the factor $\exp(-2(L - L'/L_c)^2)$ taking into account the loss of phase coherence between photons with path lengths L and L'. This effectively results in $\beta < 1$ and can impact the rate of decay of $g^2(\tau)$.For CW laser sources used in DCS>5 m, measurements, the coherence length is usually >5 m, which is much longer than the photon path lengths. In case , exp (−2) $((L\text{-}L')/LC)^2) \approx 1$, and Eq. (6) is reduced to Eq. (4) with. However, for TD-DCS, the coherence length of the laser is much shorter due to its finite spectral bandwidth (Δf) which is inversely proportional to the width of the laser pulse (Δt), i.e., $L_c\ 1/\Delta f\ \Delta t$. For a 500 ps laser, $L_e \sim 10$ cm and becomes comparable to the photon path lengths through tissue which can no longer be ignored. In addition, the path length of the detected photons is not strictly given by the sample time t_s of the detection gate because of the IRF which includes delays associated with the laser pulse and the detector response. A proper model also needs to consider the effects of the IRF.

To construct a new model, we extend the theory of Bellini for CW-DCS [16] to include the effects of the coherence length and the IRF on the intensity autocorrelation function measured from a pulsed laser with a detection gate at sample time t_S. At t_s, photons of a path length L are coming from the source at time $t_s - L/v$. We arrive at the sample time dependent intensity autocorrelation function:

$$g_2\left(t_s, \tau\right) = 1 + \int_0^\infty \mathrm{d}L \int_0^\infty \mathrm{d}L' P(L) I_p\left(t_s - L/v\right) P(L') \times I_p\left(t_s - L'/v\right) g_{1L}(L, \tau) g_{1L}(L', \tau) \exp\left(-2\left((L - L')/L_c\right)^2\right). \quad (7)$$

Here the effective path length disrtribution $P'(t_s, L) = P(L)I(t_s\text{-}L/v)$ is the path length distribution of photon trajectories measured at simple time t_s, where the normalized IRF denoted as I is included as a weighting factor. If I_P is a δ function, then is reduced to Eq. (6). For real IRFs, as we illustrate below, $P'(t_s, L)$ does not reduce to $P(t, v)$, and Eq. (7) is needed.

Examples of g2(ts, τ) computed for a Gaussian and a simu lated long-tailed IRF, which is closer to the experimental IRF we obtain with our current detectors, are plotted in Fig. 1. The width of the Gaussian IRF is 0.1 ns. The simulation parameters were set as $\mu_s' = 7\mathrm{cm}^{-1}$, μ_a=0.04 cm^{-1} ρ=1cm, λ=800×10^{-7} cm, a refractive index of the medium n=14 and R_{eff}=0.493. The path length distribution $P(L)$ and the effective path length distributions $P'(t_s$,

L) for sample times of t_s=0.2 and 1 ns, and the two IRFs, are shown in Fig. 1(b). Notice that for the long-tailed IRF, the effective path length distribution is skewed towards short photon travel times through the scattering medium. This is because the long tail of the IRF, although weak, is decaying at a comdistribution for CW-DCS measurements [black dotted curveparable rate as *P(L)*. However, compared to the path length in Fig. 1(b)], TD-DCS is still much more sensitive to long path length photons, even with the long-tailed IRF.

To compare the profiles of $g_2 t_s, \tau$ for different IRFs and coherence lengths the normalized autocorrelation functions $g_2(t_s,\tau)' = 1 + (g_2(t_s,\tau) - 1).(g_2(t_s,0) - 1)$ are plotted in Figs. 1(c) and 1(d) for t_s=0.2 and 1 ns, respectively Coherence Length and IRF have little effect on the shape of the correlation function at short t_s but, for longer t_s, the long-tailed IRF enhancement of detecting short path length photons results in a slower decay of the correlation function, which becomes even slower for the shorter coherence length. The value of β=g$_2$ (t_s, 0)-1 and the decay time t_c obtained by fitting $g_2(t_s,\tau)-1$ with a function of the form, $e^{-\tau/1}$ are plotted versus coherence length L_c decreases, β decreases as photons of different path lengths are less coherent. The effect on t_c is reduced when the IRF is symmetric, as observed for the Gaussian IRF results indicated by the solid lines in Figs. 1(e) and 1(f).

Another factor to consider in experiments is the detection gate width t_{gw} at sample time t_s. With photons arriving within a time interval t_s to $t_s + t_{gw}$, this detection gate width acts to broaden the IRF. As the model does not distinguish the IRF arising from the source or detector responses, we can simply modify the IRF to include the effect of the detection gate width by convolving I_p with a rectangular function of width t_{gw} to be the new I_p in Eq. (7). The profiles of a Gaussian pulse and convolutions with rectangular windows of t_{gw} 0.03 ns and t_{gw} 0.5 ns at t_s 0.5 ns are shown in Fig. 2(a); the effective path length distributions are shown in Fig. 2(b). The other simulation parameters are the same as in Fig. 1. Examples of $g_2'(\tau)$ for these two gate widths and L_c 1 cm and L_c 20 cm are shown in Fig. 2(c). Notice that the longer gate width results in a faster decay of the correlation function because of the detection of longer path length photons. We see in Fig. 2(d) that β decreases with increasing gate width which is consistent with previous experiments [8], and the decrease is greater for the shorter coherence length. The decay time t_c also decreases with increasing gate width.

To compare our theory with experiments, we conducted TD-DCS measurements using a homogeneous intralipid solution. The laser source (VisIR STED, PicoQuant) had a FWHM pulse width of 500 ps at 767 nm and an average power of 50 mW. Light was delivered to the sample through a 62.5 μm GRIN fiber optic cable. Diffuse photons reflected from the sample were collected with a single-mode fiber, placed 1 cm from the source fiber, and delivered to a red-enhanced single-photon avalanche diode (SPAD) detector (MPDPDM-R-FC) and measured with timing accuracy, as described in [8]. A small fraction of the laser pulse was picked off before the sample and measured by a similar SPAD to provide an estimate of the IRF. The tissue-like phanstom is a liquid mixture of 1600 ml of water. 40 ml of intralipid (10% volume fraction), and 2 ml of diluted (1:400) black India ink. At the same time as the TD-DCS measurements, we made CW-DCS and frequency domain near-infrared spectroscopy measurements using our validated MetaOx instrument connected to an external laser source of wavelength 766 nm to provide a ground truth measurement of the optical and dynamic properties of the intralipid solution [17]. The optical properties at 767 nm were found to be $\mu_s' = 5.67\mathrm{cm}^{-1}$ and μ_a 0.03 cm^{-1}. For the dynamics, BFi 1.73 × 10^{-8} cm^2/s.

The experimentally measured IRF and the TPSF obtained at ρ 1 cm are shown in Fig. 3(a). The correlation functions measured at t_s 0.06, 0.54, and 1.02 ns with a gate width $t_{gw} = 120$ ps, each averaged over a measurement time of 10 min, are shown in Fig. 3(b), and are compared with the correlation function measured with the CW-DCS system, where $\beta = 0.5$ instead of 1 due to the two polarization modes. The BFi obtained at different t_s from fitting the TD-DCS measurements using the simplistic model of Eq. (5) and our new model of Eq. (7) are shown in Fig. 3(d). The BF_i of the intralipid solution, as measured with CW-DCS, is reported for comparison. Figure 3(c) shows the coherence length estimated from the experiment and the value of β obtained from Eq. (7). The error bars are obtained by dividing the total measurement time into seven segments, each analyzed independently, to obtain the statistics. We see that the simplistic model underestimates BFi by a factor of about 2, compared with the standard estimate by CW-DCS. This is due to the long tail of the IRF which results in the detection of short path length photons at longer t_s. BFi obtained with our new model takes into account the IRF, and the results for all t_s agree with the results of the standard CW-DCS measurements. The decay of β obtained in experiments is slightly faster than the model, which likely arises from the laser used in our experiments not having a proper Gaussian frequency spectrum, as assumed in the model [16].

In conclusion, we have analyzed the effects of finite coherence length L_c and IRF on the intensity autocorrelation function $g_2 t_s, \tau$ at different time gates t_s and gate widths t_{gw}. The simplistic model of Eq. (5) is only valid if the width of the IRF is much smaller than the width of the path length distribution, so that the IRF can be considered as a δ function, and the coherence length L_c is much longer than the path length distribution width if the IRF is not a symmetric function. This is generally not feasible in experiments since L_c is proportional to the width of the pulse, so that the criterion of a narrow pulse and a long L_c cannot be satisfied simultaneously. The detailed model in Eq. (7) includes these effects and can be used to obtain accurate estimates of the tissue BFi from TD-DCS measurements. This model also provides guidance in engineering the IRF, which includes the laser pulse profile and detector responses, to obtain the desired path length distribution $P(t_s, L)$ measured at time gate t_s.

Acknowledgment.

The authors thank Picoquant and MPD for experimental components and Kimberly Stephens for help with the experiments. Any opinions, findings, conclusions, or recommendations expressed in this material are those of the author(s) and do not necessarily reflect the views of the Assistant Secretary of Defense for Research and Engineering. The authors hold patents on DCS technology.

Funding. National Institutes of Health (NIH) (R01EB025145, R01-MH111359 (DAB), R01-NS100750 (SAC), R21NS094828 (MAF)); Office of the Secretary of Defense (OSD); U.S. Air Force (USAF) (FA8721–05-C0002, FA8702–15-D-0001).

REFERENCES

1. Buckley EM, Parthasarathy AB, Grant PE, Yodh AG, and Franceschini MA, Neurophotonics 1, 011009 (2014). [PubMed: 25593978]
2. Boas DA, Campbell LE, and Yodh AG, Phys. Rev. Lett 75, 1855 (1995) [PubMed: 10060408]
3. Boas DA and Yodh AG, J. Opt. Soc. Am. A 14, 192 (1997).
4. Durduran T and Yodh AG, Neuroimage 85, 51 (2014). [PubMed: 23770408]
5. Durduran T, Yu G, Burnett MG, Detre JA, Greenberg JH, Wang J, Zhou C, and Yodh AG, Opt. Lett 29, 1766 (2004). [PubMed: 15352363]
6. Li J, Dietsche G, Iftime D, Skipetrov SE, Maret G, Elbert T, Rockstroh B, and Gisler T, J. Biomed. Opt 10, 044002 (2005).
7. Mesquita RC, Durduran T, Yu G, Buckley EM, Kim MN, Zhou C, Choe R, Sunar U, and Yodh AG, Philos. Trans. R. Soc. London Ser. A 369, 4390 (2011).
8. Sutin J, Zimmerman B, Tyulmankov D, Tamborini D, Wu KC, Selb J, Gulinatti A, Rech I, Tosi A, Boas DA, and Franceschini MA, Optica 3, 1006 (2016). [PubMed: 28008417]
9. Patterson MS, Chance B, and Wilson BC, Appl. Opt 28, 2331 (1989). [PubMed: 20555520]
10. Selb J, Joseph DK, and Boas DA, J. Biomed. Opt 11, 044008 (2006). [PubMed: 16965165]
11. Lemieux PA and Durian DJ, J. Opt. Soc. Am. A 16, 1651 (1999).
12. Pagliazzi M, Sekar SKV, Colombo L, Martinenghi E, Minnema J,Erdmann R, Contini D, Mora AD, Torricelli A, Pifferi A, and Durduran T, Biomed. Opt. Express 8, 5311 (2017). [PubMed: 29188122]
13. Pine DJ, Weitz DA, Zhu JX, and Herbolzheimer E, J. Phys. 51, 2101 (1990).
14. Boas DA, Sakadžić S, Selb JJ, Farzam P, Franceschini MA, and Carp SA, Neurophotonics 3, 031412 (2016). [PubMed: 27335889]
15. Kienle A and Patterson MS, J. Opt. Soc. Am. A 14, 246 (1997).
16. Bellini T, Glaser MA, Clark NA, and Degiorgio V, Phys. Rev. A 44, 5215 (1991). [PubMed: 9906575]
17. Carp SA,Farzam P, Redes N, Hueber DM, and Franceschini MA, Biomed. Opt. Express 8, 3993 (2017). [PubMed: 29026684]

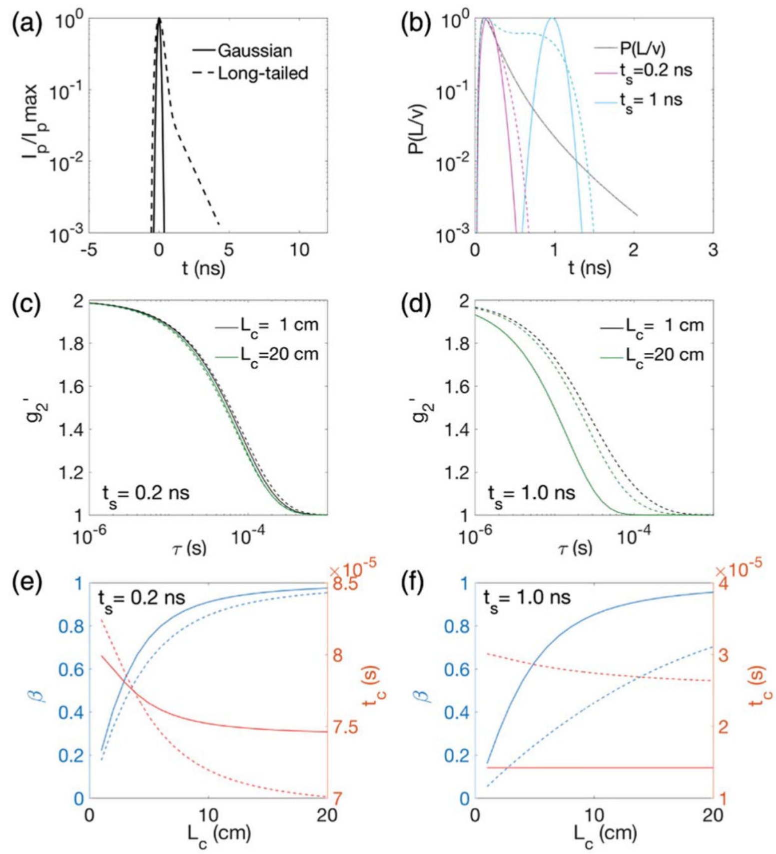

Fig. 1.

(a) Profiles of the Gaussian IRF (solid line) and the longtailed IRF (dashed line). (b) Path length distribution *P(L)*, Eq. (3), for the optical properties given in the text (dotted black line) and the effective path length distribution $P'(t_s L)$ for Gaussian (solid line) and long-tailed (dashed line) $\mathrm{IRF_s}$ at $t_s = 0.2$ ns (magenta) and $t_s = 1$ ns (cyan), versus photon travel time L/v. Normalized autocorrelation function g_2' for Gaussian (solid line) and long-tailed (dashed line) IRFs with coherence length $L_c = 1$ cm (black) and $L_c = 20$ cm (green) at (c) $t_s = 0.2$ ns and (d) at $t_s = 1$ ns. Values of β (blue) and the decay time t_c (red) of g_2' as a function of the coherence length for Gaussian (solid line) and long-tailed (dashed line) IRFs at (e) $t_s = 0.2$ ns and (f) at $t_s = 1$ ns.

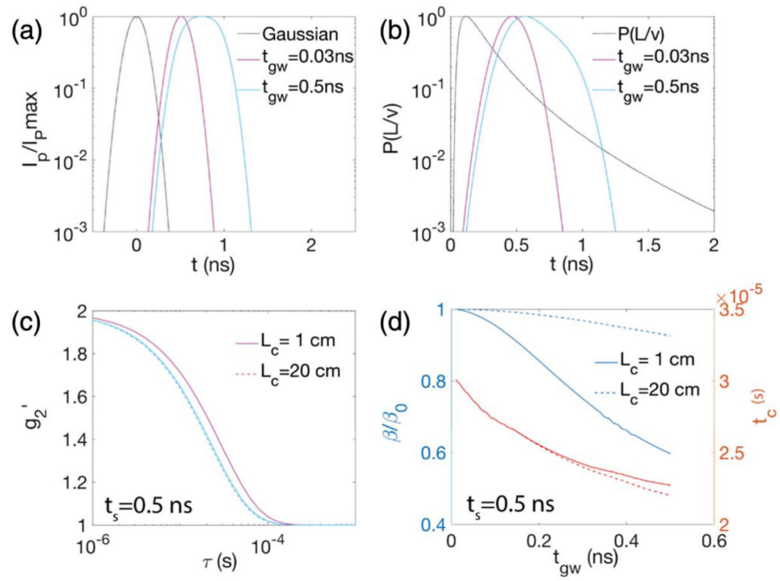

Fig. 2.

(a) Profiles of a Gaussian pulse at $t_s = 0$ (dotted black line) and IRFs of theGaussian at $t_s = 0.5$ ns convolved with a rectangular function of gate width $t_{gw} = 0.03$ ns (magenta) and $t_{gw} = 0.5$ ns (cyan). (b) Path length distribution *P(L)*, Eq. (3) (dotted black line), and the effective path length distribution $P'(t_s, L)$ for $t_{gw} = 0.03$ ns and $t_{gw} = 0.5$ ns at $t_s = 0.5$ ns), versus photon travel time L/v. (c) $g_2'$for $t_{gw} = 0.03$ ns (magenta) and $t_{gw} = 0.5$ ns (cyan) with $L_c = 1$ cm (solid line) and $L_c = 20$ cm. (d) Normalized β/β0 (blue) and decay time tc (red) for $L_c = 1$ cm (solid line) and $L_c = 20$ cm (dashed line). The values of $\beta(t_{gw} = 0)$ are 0.95 and 0.16 for $L_c = 20$ and 1 cm, respectively.

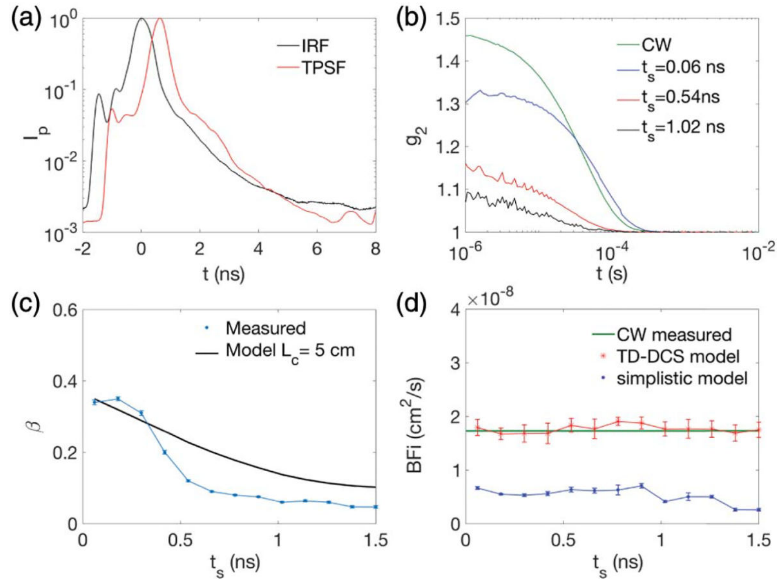

Fig. 3.

Experimental results of (a) the IRF (black) and TPSF measured at ρ 1 cm (red). (b) g_2 for the CW-DCS measurement (green) and TD-DCS measurements at t_s 0.32,0.8,1.28 ns. (c) β obtained from the experiment and the TD-DCS model in Eq. (7) with L_c 5 cm. (d) BF_is obtained from fitting using the simplistic TD-DCS model (blue) and realistic TD-DCS model (red), compared with the value obtained from the CW-DCS measurement (black). The error bars indicate standard deviations.